



## Research article

# Adsorption–photocatalysis synergy of reusable mesoporous TiO<sub>2</sub>–ZnO for photocatalytic degradation of doxycycline antibiotic

I.J. Ani<sup>a,b,d,\*</sup>, U.G. Akpan<sup>a</sup>, M.A. Olutoye<sup>a</sup>, B.H. Hameed<sup>c,\*\*</sup>, T.C. Egbosiuba<sup>e,f</sup>

<sup>a</sup> Department of Chemical Engineering, Federal University of Technology, Minna, Nigeria

<sup>b</sup> School of Chemical Engineering, University of Science Malaysia, Penang, Malaysia

<sup>c</sup> Department of Chemical Engineering, College of Engineering, Qatar University, Doha, Qatar

<sup>d</sup> Department of Chemical Engineering, Nasarawa State University, Keffi, Nigeria

<sup>e</sup> Department of Chemical Engineering, Chukwuemeka Odumegwu Ojukwu University, Uli Campus, Anambra, Nigeria

<sup>f</sup> Department of Engineering Technology and Industrial Distribution, Texas A&M University, College Station, TX, 77843, USA

## ARTICLE INFO

**Keywords:**  
Photocatalysis  
Stability  
Reusability  
Doxycycline  
Kinetic

## ABSTRACT

The potentials of mesoporous TiO<sub>2</sub>–ZnO (3TiZn) were explored on photocatalytic degradation of doxycycline (DOX) antibiotic, likewise the influence of adsorption on the photocatalytic process. The 3TiZn was characterized for physical and chemical properties. Stability, reusability, kinetic and the ability of 3TiZn to degrade high concentration of pollutant under different operating conditions were investigated. Photocatalytic degradation of DOX was conducted at varied operating conditions, and the best was obtained at 1 g/L catalyst dosage, solution inherent pH (4.4) and 50 ppm of DOX. Complete degradation of 50 ppm and 100 ppm of DOX were attained within 30 and 100 min of the reaction time, respectively. The stability and reusability study of the photocatalyst proved that at the tenth (10th) cycle, the 3TiZn is as effective in the degradation of DOX as in the first cycle. This may be attributed to the fusion of the mixed oxides during calcination. The 3TiZn is mesoporous with a pore diameter of 17 nm, and this boosts its potential to degrade high concentration of DOX. It was observed that the adsorption capacity of 3TiZn enhances the photocatalytic process. It can be emphasized that 3TiZn portrayed a remarkable catalyst stability and good potentials for industrial application.

## 1. Introduction

Antibiotics are beneficial to humans and animals, and can be detrimental to human, veterinary and eco-system [1,2]. In the mid-1990s, emerging technology informed scientists of the rising risk to humans and the eco-system associated with the discharge of antibiotics at any level of concentration [3,4]. The discharge of large effluent from pharmaceutical industries, excretion from live stocks, domestic sewage and hospitals contains antibiotics, resulting to multi-resistance bacterial strains in the eco-system which are difficult to be treated by the available drugs [3,5].

After the intake of antibiotics, it undergoes metabolism. Some of the metabolites and the unmetabolized antibiotics are excreted through urine and faeces on a large scale and thus go into water bodies [6]. A longtime exposure of organisms to antibiotics leads to health issues like light sensitivity, central nervous system damages, spermatogenesis, arthropathy, mutagenic effects, nephropathy [7].

\* Corresponding author.

\*\* Corresponding author.

E-mail addresses: [aniijeoma@nsuk.edu.ng](mailto:aniijeoma@nsuk.edu.ng) (I.J. Ani), [b.hammadi@qu.edu.qa](mailto:b.hammadi@qu.edu.qa) (B.H. Hameed).

<https://doi.org/10.1016/j.heliyon.2024.e30531>

Received 26 September 2023; Received in revised form 9 April 2024; Accepted 29 April 2024

Available online 30 April 2024

2405-8440/© 2024 Published by Elsevier Ltd. This is an open access article under the CC BY-NC-ND license (<http://creativecommons.org/licenses/by-nc-nd/4.0/>).

This calls for the need to completely mineralize the pollutant in wastewater.

Doxycycline (DOX) belongs to the family of tetracycline antibiotics consumed against gram-positive and gram-negative bacteria in both human and veterinary [8,9]. DOX consists of three functional groups such as phenolic diketone, tricarbonyl amide, and dimethylamine [9]. DOX is not bio-degradable because of its chemical stability [9,10], hence advance oxidation processes are dependable methods for the degradation of these persistent and non-biodegradable pollutants.

Heterogeneous photocatalysis; a typical advanced oxidation process (AOP) proves to be reliable for the degradation of organic pollutants [11], exhibits remarkable potentials for industrial application [12,13] and it is environmentally benign [14]. With redox reaction between the reactive radicals (RR) and organic pollutants, the pollutants are mineralized to water and carbon dioxide [15,16] or to less harmful/biodegradable pollutants. However, some setbacks are still associated with the method such as inability to degrade high concentrated pollutants, reusability and stability of photocatalysts [17], and photocatalyst recovery. Recent findings have shown how effective adsorption property of a photocatalyst can influence the degradation of a pollutants [18–21]. The quick adsorption of contaminants can boost the local concentration of contaminants on semiconductor surfaces, which can increase photocatalytic efficiency [20]. Thus, adsorption process can promote the degradation of a pollutant.

Successful degradation of DOX with UV/H<sub>2</sub>O<sub>2</sub>/Fe(III) system was achieved by the formation of complex that enabled the reduction of Fe(III) to Fe(II) at pH 3 [9], but the active ingredient (H<sub>2</sub>O<sub>2</sub>/Fe(III)) was consumed and the system can only operate in acidic medium. Also, Fenton process has been used to degrade DOX in the presence of hydrogen peroxide (H<sub>2</sub>O<sub>2</sub>) and Fe<sup>2+</sup> [22]. This process was homogenous, hence no recovery of the active ingredient for reuse. Yan et al. [12] investigated the degradation of DOX under visible light radiation with nitrogen doped graphene quantum dots-BiOI/MnNb<sub>2</sub>O<sub>6</sub> (5%NGQDs-Bi/Mn Nb<sub>2</sub>O<sub>6</sub>). In their investigation, only 67 % of 10 ppm DOX was degraded in 120 min and the catalyst was reused for four cycles. Bing et al. [23] studied the reusability of Bi<sub>2</sub>O<sub>3</sub>/Bi<sub>2</sub>WO<sub>6</sub>/MgAl-CLDH on DOX degradation which showed a slide decline in the performance of the catalyst at the fifth cycle. The stability and reusability of core-shell Ag<sub>2</sub>CrO<sub>4</sub>/N-GQDs@g-C<sub>3</sub>N<sub>4</sub> composites was investigated on the photo-degradation of DOX and the composite was stable after eight cycles tested [24]. However, to the best of our knowledge, there is no literature on photocatalytic degradation/mineralization of DOX with mesoporous TiO<sub>2</sub>-ZnO which has the potential to be reused, and stable up to ten cycles.

Semiconductor metal oxides photocatalyst gains much attention due to its ability to degrade recalcitrant organic pollutants [25]. The most stable semiconductor oxides remain TiO<sub>2</sub> and ZnO. They are suitable as pristine materials for the eradication of recalcitrant pollutants exposed to UV irradiation and are the most published work on heterogeneous photocatalysis [26,27]. ZnO absorbs wide range of UV spectrum and it has excitation binding energy at 60 meV which is quite high [28]. Under the influence of UV irradiation, it exhibits better oxidation properties, in most cases, than TiO<sub>2</sub> due to its wider range of UV spectrum absorbance [29]. Thus, complete mineralization of pollutants in wastewater is possible with the application of ZnO as photocatalyst [30]. Also, ZnO is a low toxic material that is cost effective, thermally and mechanically stable at room temperature [31]. TiO<sub>2</sub> is chemically, biologically and thermally stable, with high mechanical strength; it is cost effective and non-toxic to the ecosystem [32,33]. The TiO<sub>2</sub> and ZnO can exist as mixed oxides resulting in synergy that yield better performance than the pristine semiconductor metal oxides [2,8,34,35]. In these studies, most photocatalyst degraded less concentrated.

The challenges that limit the application of photocatalytic reactions for the treatment of real wastewater generated from industries inspired this work. This manuscript presents the effect of mesoporous 3TiZn photocatalyst on degradation of highly concentrated DOX under UV light which was enhanced by adsorption capacity of the photocatalyst. While studying the degradation of DOX by the developed mixed oxides, the study also presents the stability and reusability of the photocatalyst, which will pave a way for industrial application.

## 2. Material and methods

### 2.1. Material

Doxycycline capsule (Dynapharm), Titanium butoxide (Sigma-Aldrich), Zinc nitrate hexahydrate (R&M chemicals), Sulphuric acid (Merck), Acetic acid (R&M chemicals) and Absolute ethanol (R&M chemicals) are all analytical grade chemicals with 99.5 %, 98 %, 97 %, 98 %, 97 % and 99.8 % purity, respectively. 0.1 M HCl and 0.1 M NaOH were used to adjust the pH of the solution.

### 2.2. Preparation of photocatalyst

#### 2.2.1. Synthesis of mesoporous 3TiZn

Sol-precipitation method was used for the synthesis of TiO<sub>2</sub> using titanium butoxide as the precursor. Following the method of Morales et al. [36], a solution that contains absolute ethanol, acetic acid, titanium butoxide and H<sub>2</sub>SO<sub>4</sub> at the volume ratio of 1:0.81:0.49:0.08 was stirred at a temperature of 50°C until white precipitate was formed.

Zinc nitrate hexahydrate (97 %) was used as a precursor for synthesis of ZnO. A known amount of Zinc nitrate hexahydrate was dissolved in distilled water, followed by addition of 0.1 M NaOH to the suspension as a precipitating agent until pH12 was attained.

TiO<sub>2</sub> and ZnO precipitates in suspension were mixed at the mole ratio of 3:1 and stirred for 4 h. The suspension was filtered, washed to attain pH 7, dried at 60°C for 12 h in an oven and calcined at 650 °C. (The product of the calcined mixed oxides was named 3TiZn).

#### 2.2.2. Characterization of 3TiZn

Composition and crystallite phases of 3TiZn were investigated using X-ray diffraction (XRD) with a Philips PW 1710 in 2θ ranging

from 10° to 90°. Surface area and pore distribution of 3TiZn was determined using micromeritics ASAP 2020 model in accordance with Brunauer-Emmett-Teller (BET) method. The pore diameter and pore volume were investigated using adsorption-desorption of nitrogen using Barrett-Joyner-Halenda (BJH) model. Thermo Scientific Nicolet IS10 Fourier transform infrared (FTIR) spectrometer was used to ascertain the presence of the active functional group by the generation of FTIR from 4000 to 400 cm<sup>-1</sup>.

### 2.2.3. Photocatalytic activities on DOX

The degradation of DOX was examined over 3TiZn in a 350 mL cylindrical reactor equipped with an air bubble pump and a coolant. The reactor containing 200 mL solution was placed on a magnetic stirrer in a black box, which restricted any form of external light. The solution was stirred for 24 h at 27°C for the adsorption study in the dark without air bubble and with the photocatalyst. Thereafter, another separate reaction was carried out with a 28 W UV lamp (254 nm, jit light China), immersed in the solution, and the lamp was switched on without catalyst for the photolysis studies. Subsequently, 0.5 g/L 3TiZn photocatalyst was placed in the a separate solution in the presence of light from the lamp for the photocatalytic experiments. At different time intervals, samples of the treated solution were withdrawn and the concentration of the pollutant was determined using UV-Vis spectrophotometer (Shimadzu UV1601) at maximum absorption wavelength of DOX (254 nm). Eq. (1) was used to calculate percentage degradation.

$$C_f = \frac{C_i - C_t}{C_i} \times 100 \quad (1)$$

Where  $C_f$  = percentage degradation,  $C_i$  = initial concentration and  $C_t$  = concentration at a given time, all in ppm.

Effect of initial concentration (10–100 ppm), photocatalyst dosage (0.125–1.25 g/L) and solution pH (3–11) were studied and the data obtained from effect of initial concentration were used to determine the kinetic parameters.

### 2.2.4. Point zero charge pH ( $pH_{pzc}$ ) determination

Different pHs of solutions ranging from 2 to 11 were prepared with NaOH and HCl solution. The Initial pH of the eight solutions was recorded as  $F_i$ . 3TiZn was added to each solution with different pH value. The mass ratio of catalyst to distilled water was 0.001:1. The mixtures were agitated in a shaker for 48 h after which the final pH value ( $F_f$ ) for each mixture was recorded. A plot of  $F_i$  against  $F_f$  was used to determine point zero charge of each catalyst [37].

### 2.2.5. Determination of dominant reactive radicals

Determination of dominant reactive radicals was done by the use of radicals scavengers in the reaction. Hydroxyl radicals ( $OH^\bullet$ ) were scavenged using tert. BuOH, superoxides ( $O_2^{\bullet -}$ ) were scavenged using *p*-benzoquinone (P-BQ) and sodium iodide (NaI) was used for photo-holes ( $h^+$ ). Following the procedure used for the photocatalytic process, the investigation was done with the addition of 2 mM of each scavenger. The best operating parameters obtained for DOX during the photocatalytic study were used for the study. The generation of  $OH^\bullet$  in the solution was confirmed using Photoluminescence Spectroscopy-Terephthalic Acid (PL-TA) analysis. The same procedure for the performance analysis on 3TiZn was employed except that a solution of  $5 \times 10^{-4}$  M TA dissolved in  $2 \times 10^{-3}$  M NaOH was used instead of the DOX solution. The method of Nasura et al. [38] was used. Reaction between TA and  $OH^\bullet$  generates hydroxyterephthalic acid (HTA) which is highly fluorescent. Thus, HTA was detected by PL analysis. After the placement of the glass cuvette that contained the analyte in the in a PerkinElmer Lambda S55 spectrofluorometer for analysis, emission spectra were generated.

### 2.2.6. Reusability test

Reusability test of the photocatalyst was conducted by recycling the catalyst after each reaction. Collection of the catalyst was done by filtration after each reaction. It was dried in an oven at 60°C and reused for the next cycle, up to ten cycles tested.

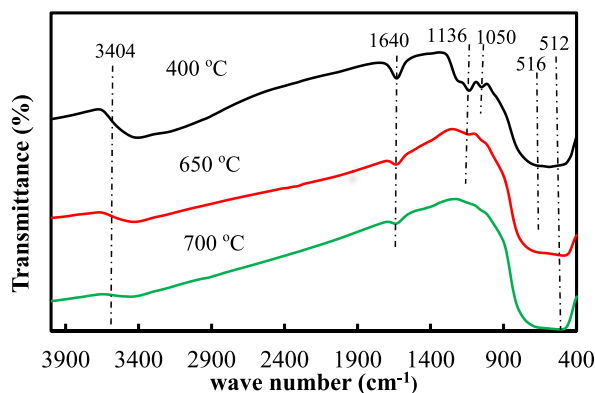


Fig. 1. FTIR spectra of mesoporous 3TiZn at different calcination temperature.

### 3. Results and discussion

#### 3.1. Characterization of mesoporous 3TiZn photocatalyst

##### 3.1.1. FTIR

The FTIR technique was used to determine the functional groups present on the surface of 3TiZn calcined at 400°C, 650°C, and 700°C and the results are presented in Fig. 1. All samples reveal peaks between 4000 and 400  $\text{cm}^{-1}$  with different alteration due to increase in calcinations temperature. The peak between 3000 and 3500  $\text{cm}^{-1}$  and 1632-1640  $\text{cm}^{-1}$  are assigned to the stretching and bending vibration of O–H group [8,39] on the surface of 3TiZn. Metal oxides exhibit absorption peaks mostly below 1000  $\text{cm}^{-1}$  [39,40] due to inter-atomic vibration or inter-metal oxygen bond in the catalyst lattice structure. Bands observed below 600  $\text{cm}^{-1}$  are ascribed to stretching vibration of the oxygen-metal linkage. Similar observation was made by Refs. [8,41]. There was a decrease in peaks at 1136-1037  $\text{cm}^{-1}$ , 1632-1640  $\text{cm}^{-1}$  and 3000-3500  $\text{cm}^{-1}$  as the calcination temperature increased (Fig. 1) and this was reflected in the photocatalyst performance. At 700°C, peaks which were observed in samples calcined at lower temperatures (400 and 650°C) between 1136 and 513  $\text{cm}^{-1}$  were eliminated, leaving only three peaks in the whole spectrum. This could be responsible for the reduction in performance of 3TiZn calcined at 700°C.

##### 3.1.2. XRD

The Phase mineralogical composition and crystallinity of the photocatalyst were determined using XRD as shown in Fig. 2. The spectrum shows very sharp peaks which depicts the crystallinity of the material. The crystal phase of  $\text{TiO}_2$  and ZnO detected were hexagonal anatase (JCPDS 00-021-1272) and hexagonal Zincite (JCPDS 00-001-1136) respectively. Also,  $\text{Zn}_2\text{Ti}_3\text{O}_8$  (JCPDS 00-013-0471) and  $\text{Zn}_2\text{TiO}_4$  (JCPDS 00-013-0536) were the Zinc titanium oxides formed during the heat treatment. The presence of Zincite was observed at 36.97, 63.2 and 67.8°, which correspond to crystal planes at 101, 103 and 112 respectively. This is similar to the result obtained by Refs. [42,43]. Anatase, which is the major composition of 3TiZn was detected at 101, 103, 200, 105, 204, 116, 215 and 224 crystal planes which corresponds with 2 $\theta$  of 25, 36.7, 48, 53.8, 62.6, 68.7, 75 and 82.6°, respectively. The strong diffraction peak of anatase at 25° was equally reported [44].  $\text{Zn}_2\text{Ti}_3\text{O}_8$  diffraction peaks were detected at 35.4, 36.8, 62.6, 70.3 and 74.3°, corresponding to crystal planes at 311, 222, 440, 620 and 622 respectively. Finally, the diffraction peaks  $\text{Zn}_2\text{TiO}_4$  corresponds with the crystal planes at 311, 222, 620 and 622. Similar crystal planes for titanate were reported [45,46].

Increase in calcination temperature of 3TiZn always lead to the formation of Zinc titanium oxide [47]. Habib et al. [48] and Wang et al. [46] equally noticed the formation of  $\text{Zn}_2\text{Ti}_3\text{O}_8$  and  $\text{Zn}_2\text{TiO}_4$  at elevated calcination temperature during the heat treatment of  $\text{TiO}_2$ -ZnO which improved the performance of their mixed oxide. Also, calcination of  $\text{TiO}_2$ -ZnO at 750 °C for 5 h led to the formation of  $\text{Zn}_2\text{Ti}_3\text{O}_8$  and  $\text{Zn}_2\text{TiO}_4$  [45]. Thus, the presence of Zinc titanium oxides at higher calcination temperature contributed to the better performance of the composite. Similar report was made by Habib et al. [48]. Average crystallite size was determined by Scherrer's equation (Eq. (2)).

$$D = \frac{0.9\lambda}{\beta \cos \theta} \quad (2)$$

D is the crystallite size;  $\beta$ ,  $\theta$  and  $\lambda$  are the line broadening, wavelength of Cu-K $\alpha$  radiation and diffraction angle respectively. Thus, the average crystallite size of the mixed oxide was determined to be 37 nm.

##### 3.1.3. Adsorption and desorption of nitrogen gas for textural analysis

Porous materials are mostly characterized according to the pore diameters/radii derived from the gas sorption data which are classified based on the IUPAC nomenclature. The adsorption and desorption of nitrogen gas under the relative pressure (P/P<sub>0</sub>) from

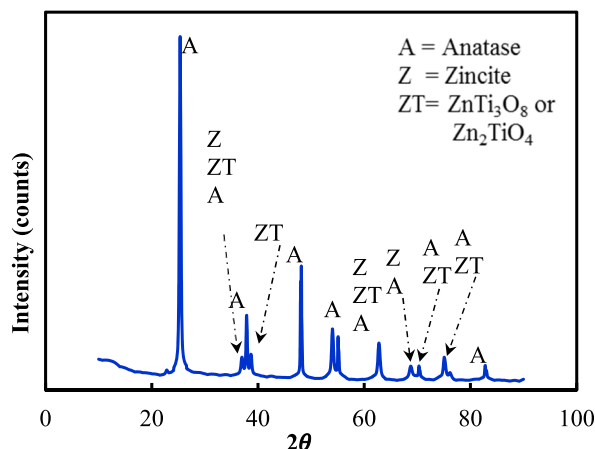


Fig. 2. XRD pattern of 3TiZn calcined at 650 °C.

0 to 0.984 provided information on the textural characteristics of the photocatalyst. Analysis on the pore size distribution and surface area of the material revealed that the photocatalyst is mesoporous with average pore diameter of 17 nm, specific surface area of  $39 \text{ m}^2/\text{g}$  and average pore volume of  $0.166 \text{ cm}^3/\text{g}$ . The hysteresis loop shown in Fig. 3(a) matches that of H3 loop with type IV isotherm (according to IUPAC classification) which represents a mesoporous material [49,50]. The average pore diameter falls within the pore diameter range for mesoporous materials (2–50 nm). Also, the uneven distribution of pores as shown in Fig. 3 (b) confirms the hysteresis loop because the material contains more of mesopores.

### 3.2. Effect of adsorption, photolysis and photocatalysis

The effect of adsorption, photolysis and photocatalysis on DOX was studied using the best operating parameters as shown in Fig. 4. The results were obtained at optimal operating conditions such as; 50 ppm of DOX, 1 g/L photocatalyst dosage and solution inherent pH. The adsorption study which was carried out for 24 h equilibrated after 30 min. Thus, adsorption study up to 60 min was reported as shown in Fig. 4. At 5, 10, 30 and 1440 min of adsorption study, 28, 26, 31 and 31 % of DOX were removed respectively. When the photocatalyst was placed in the reactor that contained DOX solution without agitation, the pollutant adhered immediately to the surface of photocatalyst, which was noticed as a result of change in colour of the photocatalyst. Thus, after 10 min of agitation, the quantity adsorbed was less than that of 5 min which could be as a result of desorption of some of the pollutant. Under photolytic study, degradation of DOX was observed which was attributed to the absorption of quantum of light which degraded the photolyte (DOX) in the absence of photocatalyst. Within 30 min of exposure of DOX to light, the reaction was very slow after which the rate of degradation increased with increase in reaction time. At 30 min, 38 % degradation was achieved whereas at 200 min, 86 % degradation was achieved. Most pharmaceuticals exhibit high absorption capacity of photons, especially UV light due to the presence of aromatic rings, heteroatoms and functional groups [51]. The absorption leads to the generation of compounds in excited electronic state that are vulnerable to degradation [51]. Thus, photolysis initiated by the absorption of photons by DOX and high adsorption capacity of 3TiZn improved the photocatalytic degradation of DOX by the generation of reactive species by the absorbed photons. During photocatalytic reaction, complete degradation was achieved at 30 min reaction time. Thus, the presence of the photocatalyst enhanced the degradation process. Xu et al. [52] carried out the photocatalytic degradation of methylene blue using metal free graphitic carbon nitride as catalyst. They reported the effect of adsorption and the decomposition behaviour of the pollutants under visible light, which improved the performance of the catalyst during photocatalytic degradation and this behaviour is exhibited in this study. Adsorption has great influence in heterogeneous photocatalysis.

### 3.3. Photocatalytic performance of 3TiZn on doxycycline degradation

#### 3.3.1. Effect of photocatalyst loading

Fig. 5(a) depicts the effect of photocatalyst loading on the degradation of DOX. Photocatalyst dosage has significant effect on pollutant degradation. Increase in dosage increased the degradation of DOX up to 1 g/L as shown in Fig. 5(a). Further increase in dosage beyond 1 g/L did not influence the degradation process. This is due to the cloudy nature of the system at such concentration which can lead to interception of light [53]. Also, increase in photocatalysts loading can lead to agglomeration of the photocatalyst. Klauson et al. [7] experienced the same behaviour with 1.5 g/L photocatalyst dosage during the degradation of DOX, likewise Nuengmarcha et al. [54]. Thus, the best dosage was chosen to be 1 g/L in this study.

#### 3.3.2. Effect of initial concentration of DOX

Effect of initial concentration on the degradation of DOX by 3TiZn (Fig. 5(b)) was investigated. Increase in initial concentration decreased the degradation capacity of the photocatalyst as a result of lack of direct contact between the pollutants and the active sites due to limited number of 3TiZn active sites or deactivation of the active sites. Furthermore, the photons have limited access to the

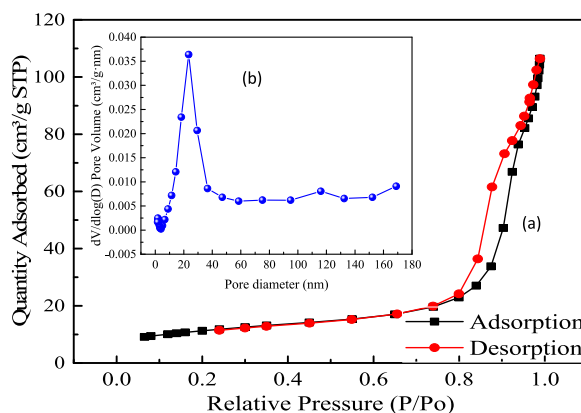


Fig. 3. (a) Nitrogen Adsorption-desorption isotherm (b) pore size distribution.

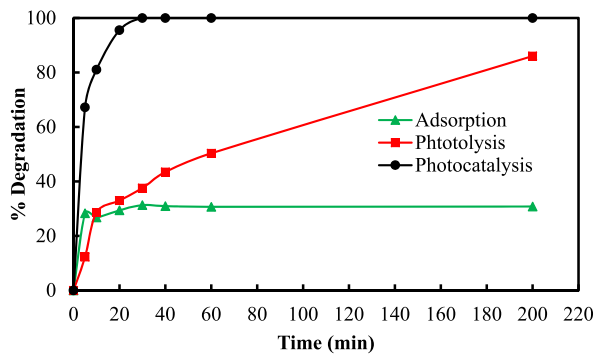


Fig. 4. Effect of adsorption, photolysis and photocatalysis on DOX at 50 ppm, solution inherent pH and 1 g/L.

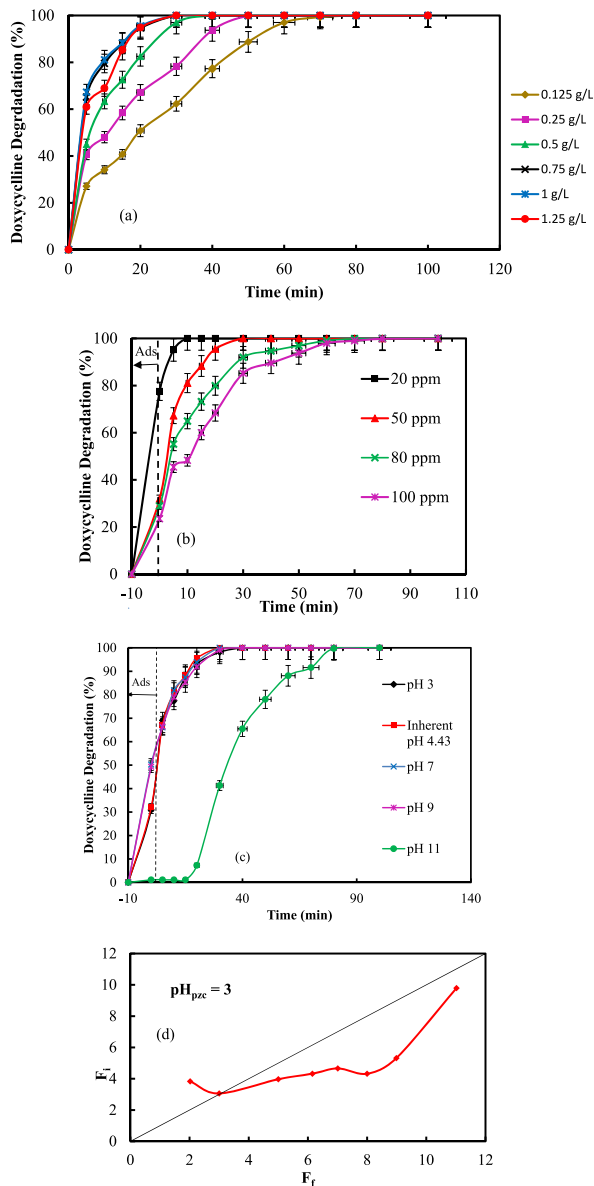


Fig. 5. (a) Effect of 3TiZn loading on DOX ( $C_{doxo} = 50$  ppm and solution inherent pH); (b) Effect initial concentration at 1 g/L and solution inherent pH; (c) Effect of pH on photocatalytic degradation of DOX ( $C_{doxo} = 50$  ppm, 1 g/L); (d)  $pH_{PZC}$  determination; Plot of initial pH ( $F_i$ ) vs final pH ( $F_f$ ).

active sites thereby affecting the generation of the active radicals [29]. As shown in Figs. 5(b), 78 % of 20 ppm was removed during adsorption study after 10 min of contact time; likewise, almost 100 % of 10 ppm was removed by adsorption. Thus, initial concentration at 10 ppm was not inclusive and that 20 ppm was not considered as the best either, because the removal of the pollutant was more of adsorption than photocatalysis and this study is focused on photocatalysis. For that of 50, 80 and 100 ppm, 32, 28 and 23 % of DOX were adsorbed respectively. Thus, chemical reaction is the dominant mechanism for the DOX degradation than adsorption mechanism. 3TiZn can degrade higher concentration of DOX up to 100 ppm studied. At 10 min, complete degradation was observed for 20 ppm DOX, and then it took 30, 80 and 100 min for 50, 80 and 100 ppm to attained complete degradation.

It can be observed in Fig. 5(b) that the high adsorption capacity of 3TiZn improved the photocatalytic degradation of DOX due to its high mesoporous nature. Mesoporous materials have inherent interconnected pore networks that helps to efficiently transport molecules to active sites [40]. Also, there is a balance between adsorption and photocatalysis. If the adsorption capacity were to be too high, it will lead to obstruction of the active sites by the pollutant molecules and prevent penetration of photons resulting to little or no generation of active radicals. However, if there was little or no adsorption capacity, there is degradation at slow rate because the active radicals have to migrate from the catalyst surface to the bulk liquid, which may take longer time to act on the pollutants. A mesoporous  $\text{TiO}_2$ , synthesized with a template (F127; triblock copolymer surfactant) has shown remarkable difference in performance for the photocatalytic degradation of organic pollutants in comparison with commercial  $\text{TiO}_2$  [55]. Similar findings were equally revealed in literature whereby sulphuric acid induced mesoporous  $\text{TiO}_2$  was used for the photocatalytic degradation of methylene blue which showed better performance than commercial  $\text{TiO}_2$  [56]. However, in this study, a template free mesoporous 3TiZn was synthesized and employed. Also, the crystallinity of the photocatalyst enhanced the photocatalytic reaction.

### 3.3.3. Effect of initial pH of solution

The influence of initial solution pHs and a plot of point zero charge of 3TiZn are shown in Fig. 5(c) and (d) respectively. DOX is a compound that can exist as cationic ( $\text{DCH}_3^+$ ), zwitterionic ( $\text{DCH}_2$ ) or anionic ( $\text{DCH}^-$  and  $\text{DC}^{2-}$ ) [9]. In acidic medium it can protonated; at neutral medium (pH 7), DOX deprotonates. Double deprotonation occurs under alkaline medium [9,57]. Thus, the solution's inherent pH and the surface pH of the catalyst are highly influential in the photocatalytic degradation of DOX.

Effect of pH at 3, 4.43 (solution inherent pH), 7, 9 and 11 were studied. From results shown in Fig. 5(c), the best degradation percentage of 50 ppm DOX via UV irradiation was at pH 4.43 (100 %), pH 7 (100 %) and pH 9 (99 %), followed by pH 3 (98 %) and pH 11 (41 %), all within 30 min of irradiation time. At pH 3, there might have been columbic repulsion between the protonated DOX and the photocatalyst with point of zero charge of 3 as shown in Fig. 5(d). Increase in pH was more favourable due to deprotonation of DOX which promoted adsorption of DOX. At pH 11, DOX became double deprotonated [9,58], likewise the photocatalyst, due to the reaction between OH from NaOH and 3TiZn. Thus, the reduction in photodegradation is as a result of repulsion between the double deprotonated DOX and negatively charged 3TiZn which led to absence of adsorption, hence no reaction.

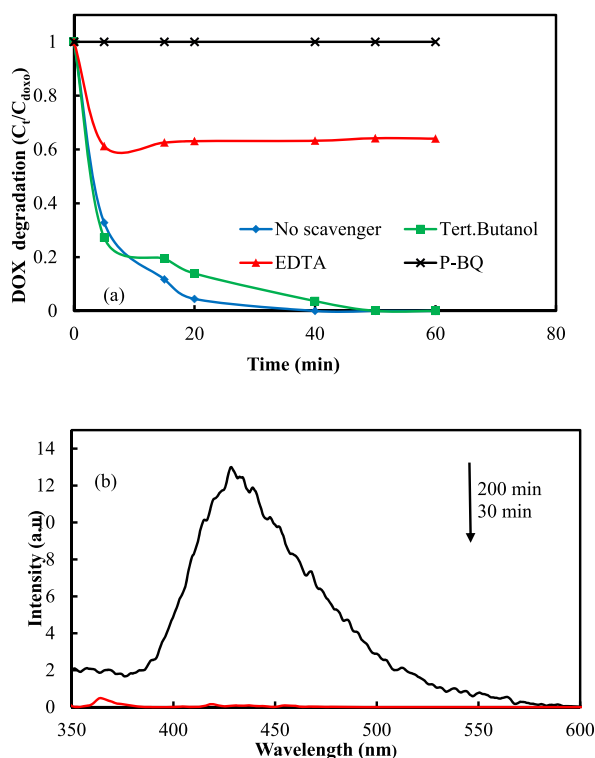


Fig. 6. (a) Determination of dominant radical; (b) PL-TA analysis for the detection of  $\text{OH}^\bullet$

However, at 20 min, the  $\text{OH}^-$  generated appeared to have been used up by  $\text{h}^+$  to produce  $\text{OH}^\bullet$ , thereby giving rise to reaction (Eq. (3)) and this is in conformity with previous literature [53,59]. As the reaction progressed, the dominant radical ( $\text{O}_2^{\bullet-}$ ) was generated along with  $\text{h}^+$  which led to the degradation of DOX. With the scavenger analyses carried out to detect the active radicals as shown in Fig. 6(a), it was confirmed that the most active radicals are  $\text{O}_2^{\bullet-}$  and  $\text{h}^+$ . Thus, this could be the reason why at the first 15 min of reaction (Fig. 5(c)), the generated  $\text{OH}^\bullet$  could not degrade DOX at pH 11. Effect of pH study at pH 11 appears to be the only reaction whereby there was no adsorption, only reaction was observed after 20 min of the irradiation. Complete degradation was attained within 80 min at pH 11. The solution inherent pH was chosen to be the best because the photocatalyst was highly reusable at the solution inherent pH. Klauson et al. [7] obtained their best pH at the inherent pH of the DOX solution using commercial P25  $\text{TiO}_2$ , which is similar to the best pH obtained in this study.

The absorption peak at 425 nm formed as a result of the reaction between  $\text{OH}^\bullet$  and TA (Fig. 6(b)) attest to the presence of HTA. This proves that there was separation of electrons and holes, hence the formation of  $\text{OH}^\bullet$ . As time increased, the concentration of  $\text{OH}^\bullet$  increased which reflects on the intensity of the peak. This confirms the presence of  $\text{OH}^\bullet$  in the solution. However, it was not the species that influenced the degradation process.



### 3.4. Reusability study

Fig. 7 shows the findings on the reusability study. 3TiZn was studied to verify its potentials for industrial application. The photocatalyst was able to degrade 50 ppm DOX for 10 cycles investigated and still has the ability to go beyond. This is an evidence of absence of deactivated active sites. In photocatalysis, the major reason for instability of catalyst is the deactivation of the active site by leaching of the active component of the catalyst or the blockage of active sites by intermediates or the parent pollutants. In the latter case, it can easily occur with a photocatalyst with very high adsorption capacity. One of the main properties of 3TiZn that is responsible for its reusability and stability is the fusion of the mixed oxides during calcination, leading to the formation of zinc titanium oxides. He et al. [60] made similar observation, whereby ZnO/Zinc titanate, calcined at 700°C, was stable and reusable for the photo-degradation of methylene blue. In this study, at 30 min, 100% degradation of DOX was attained but the colour of the photocatalyst still shows the presence of intermediates on it. Thus, in order to achieve effective reusability and stability, the reaction time was extended to 45 min to clear the surface of 3TiZn in order to adsorb subsequent DOX and intermediates. With this adjustment in reaction time, 3TiZn was stable and reusable up to ten (10) cycles tested. At 10th cycle, 99.98 % degradation of DOX was achieved within 45 min.

It must be noted that stability and reusability of a photocatalyst is one of the critical perspectives to consider in the development/design of the photocatalyst and this is very important for its industrial application. Also, ability of 3TiZn to degrade high concentration pollutant was demonstrated in this study and it is paramount for its application in real wastewater.

### 3.5. Comparative study on photocatalytic degradation of DOX

A comparative study was carried out on the performance of 3TiZn with other photocatalysts reported in literature for photocatalytic degradation of DOX (Table 1). The tremendous performance shown by 3TiZn is as result of the mesoporous nature of the catalyst, the fusion of the metal oxides during calcination and effective separation of photo-generated electrons and holes.

### 3.6. Kinetic study

The kinetic parameters for DOX photocatalytic degradation at various initial concentrations of the pollutant were evaluated which are presented in Table 2. Plot of  $\ln(C_{\text{doxo}}/C_{\text{dox}})$  against time (Eq. (4)) was used to determine apparent rate constant ( $k_{\text{app}}$ ). The

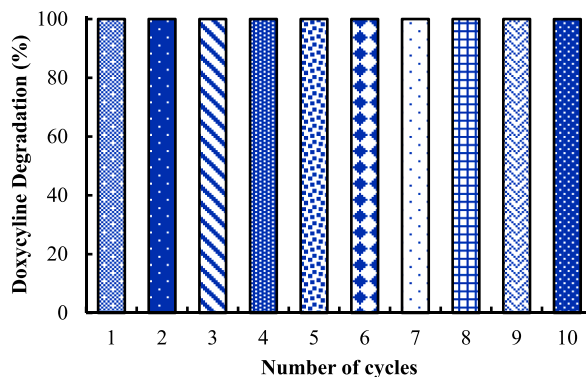


Fig. 7. Reusability and stability test on 3TiZn at 1 g/L 3TiZn dosage, 50 ppm DOX within 45 min.

**Table 1**  
A comparative study on DOX photocatalytic degradation.

Catalyst	Method	Co/Dosage	S.pH	Light	Degradation (%) / Time	Reusability	Ref.
3TiZn	Photocatalysis	50 ppm/1 g/L	Natural (4.4)	UVC	100/20 min	10	This study
5%g-C <sub>3</sub> N <sub>4</sub> @ CeO <sub>2</sub>	Photocatalysis	10 ppm/1 g/L, 100 μL H <sub>2</sub> O <sub>2</sub>	NA	Visible (150 W)	84/60 min	4	[61]
BiOBr/FeWO <sub>4</sub>	Photocatalysis	NA/1 g/L	NA	Visible (300 W)	90/1 h	4	[62]
Pd-TiO <sub>2</sub>	Photocatalysis	25 ppm/1 g/L	NA	UVA (15W)	100/15 min	–	[63]
H <sub>2</sub> O <sub>2</sub> /Fe (III)	Fenton-based	10 μM/100 μM (Fe (III), 10 μM/(H <sub>2</sub> O <sub>2</sub> ))	3	UVC	100/<20 min	–	[9]
NGQDs-BiOI/MnNb <sub>2</sub> O <sub>6</sub>	Photocatalysis	10 ppm/0.5 g/L	NA	Visible (250 W)	65.7/120 min	–	[12]
ZnO	Photocatalysis	10 ppm/0.25 g/L	10	UVC	100/5 h	–	[57]
CoFe <sub>2</sub> O <sub>4</sub> /H <sub>2</sub> O <sub>2</sub>	Heterogeneous fenton	20 ppm/1.5 g/L, 10 mM (H <sub>2</sub> O <sub>2</sub> )	6.5	–	92/10 min	5	[64]
TiO <sub>2</sub> -MCM-41	Photocatalysis	30 μM/1.5 g/L	6	UVC	>270 min	–	[65]
ZnIn <sub>2</sub> S <sub>4</sub> /NiFe <sub>2</sub> O <sub>4</sub> /biochar	Photocatalysis	30 ppm/0.5 g/L	5	Simulated sunlight	94/120 min	6	[66]
modified g-C <sub>3</sub> N <sub>4</sub> /MgZnA	Adsorption-photocatalysis	10 ppm/0.5 g/L	–	Visible light	91.46/120 min	–	[67]
Fe/Pr <sub>6</sub> O11–MoO <sub>3</sub> @g-C <sub>3</sub> N <sub>4</sub> NCs	Photocatalysis	50 ppm/0.05 g/L	7	Visible light	98/220 min	6	[68]

experimental data were fitted to pseudo-first-order kinetic reaction due to high value of the correlation coefficient ( $R^2$ ) obtained. The  $k_{app}$  obtained for various initial concentrations ( $C_{Doxo}$ ) of 20, 50, 80 and 100 ppm are 1.1646, 0.104, 0.483 and 0.0235/min respectively. It was difficult to evaluate the constant for concentrations of 10 ppm because the photocatalytic reaction took place within a very short time interval. Thus, the apparent rate constant was determined for reactions at initial concentrations of 20, 50, 80 and 100 ppm.

$$\ln\left(\frac{C_{doxo}}{C_{dox}}\right) = k_{app}t \quad (4)$$

Since adsorption can be involved in photocatalytic reaction, it was necessary to establish the dominant process (adsorption or reaction) that is responsible for the removal of DOX, which can be verified efficiently with Langmuir-Hinshelwood (L-H) model (Eq. (5)).

$$r = k_r\theta = -\frac{dC}{dt} = -k_r \frac{K_a C}{1 + K_a C} \quad (5)$$

where  $r$  is the reaction rate (mol/L/min),  $\theta$  is the occupied fraction sites,  $k_r$  is the surface reaction rate constant (mol/L/min),  $K_a$  (L/mg) is the equilibrium constant for adsorption of pollutants on 3TiZn and  $C$  is the pollutants concentration at time  $t$ , the duration of the degradation process (mol/L). Linearizing L-H model, by taking a reciprocal of both sides of Eq. (5), yields Eq. (6).

$$\frac{1}{r} = \frac{1 + K_a C}{k_r K_a C} = \frac{1}{k_r} + \frac{1}{k_r K_a C} \quad (6)$$

The plot of  $1/r$  vs  $1/C$  (Fig. 8) was used to generate  $k_r$  and  $K_a$  for DOX. The obtained  $k_r$  value (6.1350) was greater than  $K_a$  (0.0264). This indicates that DOX removal was more of reaction than adsorption which is desirable in photocatalytic activities.

#### 4. Conclusion

Mesoporous 3TiZn was effectively developed for the photocatalytic degradation of DOX under UV irradiation. It demonstrated the ability to degrade 100 ppm DOX at 100 min completely with photocatalyst dosage of 1 g/L which is due to the mesoporous nature of the material. It is reusable and stable up to 10 cycles investigated over 50 ppm DOX. The catalyst colour remained unchanged after the 10th cycle of use which reveals its stability to undergo more than 10 cycles. Calcination of 3TiZn at temperature  $>650^\circ\text{C}$  could lead to collapse of catalyst pore walls which is not favourable to the performance of the photocatalyst. Fused composites can enhance the stability and reusability of a photocatalyst. It can prevent deactivation or poisoning of photocatalyst active sites. The developed photocatalyst possesses qualities that can degrade and mineralize persistent and non-biodegradable pollutants which could make the treated water recyclable/reusable in industries or environmentally benign when discharged after treatment. The adsorption property of the photocatalyst influenced its ability to degrade high concentrated DOX. Hence, 3TiZn can be recommended for treatment of real pharmaceutical wastewater. Functionalization of the photocatalyst is recommended so as to make it multi-functional to enable its application on complex real wastewater.

**Table 2**  
Kinetic parameters for the degradation of DOX using 3TiZn.

Initial concentration (ppm)	$K_{app}/min$	$R^2$
20	1.1646	0.9187
50	0.104	0.955
80	0.483	0.9956
100	0.0235	0.9707

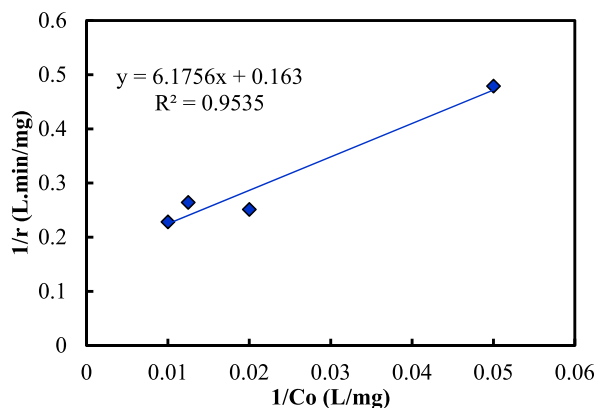


**Fig. 8.** Plots of  $1/r$  against  $1/Co$  for DOX under UV light using 3TiZn.

#### Data availability statement

A thesis with the data has been uploaded to Federal University of Technology, Minna, Nigeria repository for Turnitin similarity index check.

#### CRediT authorship contribution statement

**L.J. Ani:** Writing – original draft, Methodology, Conceptualization. **U.G. Akpan:** Conceptualization, Data curation, Formal analysis, Investigation, Methodology, Supervision, Validation, Writing – review & editing. **M.A. Olutoye:** Methodology, Project administration, Resources, Supervision, Validation, Writing – review & editing. **B.H. Hameed:** Investigation, Methodology, Resources, Supervision, Validation, Writing – review & editing. **T.C. Egbosiuba:** Data curation, Formal analysis, Investigation, Methodology.

#### Declaration of competing interest

The authors declare that they have no known competing financial interests or personal relationships that could have appeared to influence the work reported in this paper.

#### References

- [1] J. Zhu, S. Liu, Q. Yang, P. Xu, J. Ge, X. Guo, Fabrication of flower-like Ag@AgCl/Bi<sub>2</sub>WO<sub>6</sub> photocatalyst and its mechanism of photocatalytic degradation, *Colloids Surf. A Physicochem. Eng. Asp.* 489 (2016) 275–281, <https://doi.org/10.1016/j.colsurfa.2015.11.009>.
- [2] N.G. Menon, S.S. V. Tatiparti, S. Mukherji, Synthesis, characterization and photocatalytic activity evaluation of TiO<sub>2</sub>–ZnO nanocomposites: elucidating effect of varying Ti:Zn molar ratio, *Colloids Surf. A Physicochem. Eng. Asp.* 565 (2019) 47–58, <https://doi.org/10.1016/j.colsurfa.2018.12.053>.
- [3] H. Xiong, D. Zou, D. Zhou, S. Dong, J. Wang, B.E. Rittmann, Enhancing degradation and mineralization of tetracycline using intimately coupled photocatalysis and biodegradation (ICPB), *Chem. Eng. J.* 316 (2017) 7–14, <https://doi.org/10.1016/j.cej.2017.01.083>.
- [4] V. Homem, L. Santos, Degradation and removal methods of antibiotics from aqueous matrices - a review, *J. Environ. Manag.* 92 (2011) 2304–2347, <https://doi.org/10.1016/j.jenvman.2011.05.023>.
- [5] L. Zhang, W. Ding, J. Qiu, H. Jin, H. Ma, Z. Li, D. Cang, Modeling and optimization study on sulfamethoxazole degradation by electrochemically activated persulfate process, *J. Clean. Prod.* 197 (2018) 297–305, <https://doi.org/10.1016/j.jclepro.2018.05.267>.
- [6] M. Kaur, S.K. Mehta, S.K. Kansal, Visible light driven photocatalytic degradation of ofloxacin and malachite green dye using cadmium sulphide nanoparticles, *J. Environ. Chem. Eng.* 6 (2018) 3631–3639, <https://doi.org/10.1016/j.jece.2017.04.006>.
- [7] D. Klauseon, A. Poljakova, N. Pronina, M. Krichevskaya, A. Moiseev, T. Dedova, S. Preis, Aqueous photocatalytic oxidation of doxycycline, *J. Adv. Oxid. Technol.* 16 (2013) 234–243, <https://doi.org/10.1515/jaots-2013-0203>.
- [8] B. Boro, B.M. Samdarshi, S.K. Rajbongshi, Synthesis and fabrication of TiO<sub>2</sub>–ZnO nanocomposite based solid state dye sensitized solar cell, *J. Mater. Sci. Mater. Electron.* 27 (2016) 9929–9940, <https://doi.org/10.1007/s10854-016-5062-8>.
- [9] J. Bolobajev, M. Trapido, A. Goi, Effect of iron ion on doxycycline photocatalytic and Fenton-based autocatalytic decomposition, *Chemosphere* 153 (2016) 220–226, <https://doi.org/10.1016/j.chemosphere.2016.03.042>.
- [10] X.Y. Hu, K. Zhou, B.Y. Chen, C.T. Chang, Graphene/TiO<sub>2</sub>/ZSM-5 composites synthesized by mixture design were used for photocatalytic degradation of oxytetracycline under visible light: mechanism and biotoxicity, *Appl. Surf. Sci.* 362 (2016) 329–334, <https://doi.org/10.1016/j.japsusc.2015.10.192>.

- [11] V.G. Dileepkumar, P.S. Surya, C. Pratap Kumar, R. Viswanatha, C.R. Ravikumar, M.R. Anil Kumar, H.B. Muralidhara, I.M. Al-Akraa, A.M. Mohammad, Z. Chen, X.-T. Bui, M.S. Santosh, NaFeS<sub>2</sub> as a new photocatalytic material for the degradation of industrial dyes, *J. Environ. Chem. Eng.* 8 (2020) 104005, <https://doi.org/10.1016/j.jece.2020.104005>.
- [12] M. Yan, Y. Hua, F. Zhu, W. Gu, J. Jiang, H. Shen, W. Shi, Fabrication of nitrogen doped graphene quantum dots-BiO<sub>1</sub>/MnNb<sub>2</sub>O<sub>6</sub> p-n junction photocatalysts with enhanced visible light efficiency in photocatalytic degradation of antibiotics, *Appl. Catal., B* 202 (2017) 518–527, <https://doi.org/10.1016/j.apcatb.2016.09.039>.
- [13] U.G. Akpan, B.H. Hameed, Photocatalytic degradation of 2,4-dichlorophenoxyacetic acid by Ca-Ce-W-TiO<sub>2</sub> composite photocatalyst, *Chem. Eng. J.* 173 (2011) 369–375, <https://doi.org/10.1016/j.cej.2011.07.069>.
- [14] M.D.G. De Luna, L.K.B. Paragas, R.-A. Doong, Insights into the rapid elimination of antibiotics from aqueous media by tunable C<sub>3</sub>N<sub>4</sub> photocatalysts: effects of dopant amount, co-existing ions and reactive oxygen species, *Sci. Total Environ.* 669 (2019) 1053–1061, <https://doi.org/10.1016/j.scitotenv.2019.03.003>.
- [15] I.J. Ani, U.G. Akpan, M.A. Olutoye, B.H. Hameed, Solar light responsive TiO<sub>2</sub>-ZnO, modified with graphitic carbon nitride nano-sheet for degradation of AB29, *J. Chem. Technol. Biotechnol.* (2020), <https://doi.org/10.1002/jctb.6439>.
- [16] A.S. Yusuff, K.A. Bello, T.M. Azeez, Photocatalytic degradation of an anionic dye in aqueous solution by visible light responsive zinc oxide-termites hill composite, *React. Kinet. Mech. Catal.* 131 (2020) 537–554, <https://doi.org/10.1007/s11144-020-01839-z>.
- [17] P. Bansal, A. Verma, Pilot-scale single-step reactor combining photocatalysis and photo-Fenton aiming at faster removal of Cephalixin, *J. Clean. Prod.* 195 (2018) 540–551, <https://doi.org/10.1016/j.jclepro.2018.05.219>.
- [18] Y. Yu, H. Huang, Coupled adsorption and photocatalysis of g-C<sub>3</sub>N<sub>4</sub> based composites: material synthesis, mechanism, and environmental applications, *Chem. Eng. J.* 453 (2023) 139755, <https://doi.org/10.1016/j.cej.2022.139755>.
- [19] Y. Yu, X. Hu, M. Li, J. Fang, C. Leng, X. Zhu, W. Xu, J. Qin, L. Yao, Z. Liu, Z. Fang, Constructing mesoporous Zr-doped SiO<sub>2</sub> onto efficient Z-scheme TiO<sub>2</sub>/g-C<sub>3</sub>N<sub>4</sub> heterojunction for antibiotic degradation via adsorption-photocatalysis and mechanism insight, *Environ. Res.* 214 (2022) 114189, <https://doi.org/10.1016/j.envres.2022.114189>.
- [20] Q. Tian, Q. Yang, W. Guo, X. Li, G. Fang, Y. Ge, X. Liu, H. Yin, A. Pan, N. Li, Synergy of adsorption-photocatalysis and enriched surface oxygen vacancies over lignin-biochar/Bi<sub>2</sub>MoO<sub>6</sub> nanocomposites for organic pollutant removal and bamboo ECF bleaching effluent treatment, *Ind. Crops Prod.* 191 (2023) 115966, <https://doi.org/10.1016/j.indcrop.2022.115966>.
- [21] S. Lu, Y. Ma, L. Zhao, Production of ZnO-CoOx-CeO<sub>2</sub> nanocomposites and their dye removal performance from wastewater by adsorption-photocatalysis, *J. Mol. Liq.* 364 (2022) 119924, <https://doi.org/10.1016/j.molliq.2022.119924>.
- [22] A.A. Borghi, M.F. Silva, S. Al Arni, A. Converti, M.S.A. Palma, Doxycycline degradation by the oxidative Fenton process, *J. Chem.* 2015 (2015) 1–9, <https://doi.org/10.1155/2015/492030>.
- [23] X. Bing, J. Li, J. Liu, X. Cui, F. Ji, Biomimetic synthesis of Bi<sub>2</sub>O<sub>3</sub>/Bi<sub>2</sub>WO<sub>6</sub>/Mg/Al-CLDH hybrids from lotus pollen and their enhanced adsorption and photocatalysis performance, *J. Photochem. Photobiol. Chem.* 364 (2018) 449–460, <https://doi.org/10.1016/j.jphotochem.2018.06.030>.
- [24] C. Feng, Y. Deng, L. Tang, G. Zeng, J. Wang, J. Yu, Y. Liu, B. Peng, H. Feng, J. Wang, Core-shell Ag<sub>2</sub>CrO<sub>4</sub>/N-GQDs@g-C<sub>3</sub>N<sub>4</sub> composites with anti-photocorrosion performance for enhanced full-spectrum-light photocatalytic activities, *Appl. Catal., B* 239 (2018) 525–536, <https://doi.org/10.1016/j.apcatb.2018.08.049>.
- [25] S. Yin, W. Fan, J. Di, T. Wu, J. Yan, M. He, J. Xia, H. Li, La<sup>3+</sup> doped BiOBr microsphere with enhanced visible light photocatalytic activity, *Colloids Surf. A Physicochem. Eng. Asp.* 513 (2017) 160–167, <https://doi.org/10.1016/j.colsurfa.2016.10.012>.
- [26] J. Wen, J. Xie, X. Chen, X. Li, A review on g-C<sub>3</sub>N<sub>4</sub>-based photocatalysts, *Appl. Surf. Sci.* 391 (2017) 72–123, <https://doi.org/10.1016/j.apsusc.2016.07.030>.
- [27] M.R.D. Khaki, M.S. Shafeeyan, A.A.A. Raman, W.M.A.W. Daud, Evaluating the efficiency of nano-sized Cu doped TiO<sub>2</sub>/ZnO photocatalyst under visible light irradiation, *J. Mol. Liq.* 258 (2018) 354–365, <https://doi.org/10.1016/j.molliq.2017.11.030>.
- [28] V.A. Coleman, C. Jagadish, Basic properties and applications of ZnO, in: *Zinc Oxide Bulk, Thin Films and Nanostructures*, 2006, pp. 1–20, <https://doi.org/10.1016/B978-008044722-3/50001-4>.
- [29] I.J. Ani, U.G. Akpan, M.A. Olutoye, B.H. Hameed, Photocatalytic degradation of pollutants in petroleum refinery wastewater by TiO<sub>2</sub>- and ZnO-based photocatalysts: recent development, *J. Clean. Prod.* 205 (2018) 930–954, <https://doi.org/10.1016/j.jclepro.2018.08.189>.
- [30] M. Ahmad, E. Ahmed, F. Zafar, N.R. Khalid, N.A. Niaz, A. Hafeez, M. Ikram, M.A. Khan, Z. Hong, Enhanced photocatalytic activity of Ce-doped ZnO nanoparticles synthesized by combustion method, *J. Rare Earths* 33 (2015) 255–262, [https://doi.org/10.1016/S1002-0721\(14\)60412-9](https://doi.org/10.1016/S1002-0721(14)60412-9).
- [31] A.W. Skinner, A.M. DiBernardo, A.M. Masud, N. Aich, A.H. Pinto, Factorial design of experiments for optimization of photocatalytic degradation of tartrazine by zinc oxide (ZnO) nanorods with different aspect ratios, *J. Environ. Chem. Eng.* 8 (2020) 104235, <https://doi.org/10.1016/j.jece.2020.104235>.
- [32] U.G. Akpan, B.H. Hameed, Enhancement of the photocatalytic activity of TiO<sub>2</sub> by doping it with calcium ions, *J. Colloid Interface Sci.* 357 (2011) 168–178, <https://doi.org/10.1016/j.jcis.2011.01.014>.
- [33] K.H. Rahman, A.K. Kar, Effect of band gap variation and sensitization process of polyaniline (PANI)-TiO<sub>2</sub> p-n heterojunction photocatalysts on the enhancement of photocatalytic degradation of toxic methylene blue with UV irradiation, *J. Environ. Chem. Eng.* (2020) 104181, <https://doi.org/10.1016/j.jece.2020.104181>.
- [34] P. Cheng, Y. Wang, L. Xu, P. Sun, Z. Su, F. Jin, F. Liu, Y. Sun, G. Lu, High specific surface area urchin-like hierarchical ZnO-TiO<sub>2</sub> architectures: hydrothermal synthesis and photocatalytic properties, *Mater. Lett.* 175 (2016) 52–55, <https://doi.org/10.1016/j.matlet.2016.03.120>.
- [35] M.I. Khan, K.A. Bhatti, R. Qindeel, L.G. Bousiakou, N. Alonizan, Investigations of the structural, morphological and electrical properties of multilayer ZnO/TiO<sub>2</sub> thin films, deposited by sol-gel technique, *Results Phys.* 6 (2016) 156–160, <https://doi.org/10.1016/j.rinp.2016.01.015>.
- [36] J. Morales, A. Maldonado, M.D.L.L. Olvera, Synthesis and characterization of nanostructured TiO<sub>2</sub> anatase-phase powders obtained by the homogeneous precipitation method. 2013 10th International Conference on Electrical Engineering, Computing Science and Automatic Control, 2013, pp. 391–394, <https://doi.org/10.1109/ICEEE.2013.6676015>. CCE 2013.
- [37] M. Pashai Gatabi, H. Milani Moghaddam, M. Ghorbani, Point of zero charge of maghemite decorated multiwalled carbon nanotubes fabricated by chemical precipitation method, *J. Mol. Liq.* 216 (2016) 117–125, <https://doi.org/10.1016/j.molliq.2015.12.087>.
- [38] N. Nasuha, S. Ismail, B.H. Hameed, Activated electric arc furnace slag as an effective and reusable Fenton-like catalyst for the photodegradation of methylene blue and acid blue 29, *J. Environ. Manag.* 196 (2017) 323–329, <https://doi.org/10.1016/j.jenvman.2017.02.070>.
- [39] U.G. Akpan, B.H. Hameed, Solar degradation of an azo dye, acid red 1, by Ca-Ce-W-TiO<sub>2</sub> composite catalyst, *Chem. Eng. J.* 169 (2011) 91–99, <https://doi.org/10.1016/j.cej.2011.02.058>.
- [40] R. Hao, G. Wang, H. Tang, L. Sun, C. Xu, D. Han, Template-free preparation of macro/mesoporous g-C<sub>3</sub>N<sub>4</sub>/TiO<sub>2</sub> heterojunction photocatalysts with enhanced visible light photocatalytic activity, *Appl. Catal., B* 187 (2016) 47–58, <https://doi.org/10.1016/j.apcatb.2016.01.026>.
- [41] U.G. Akpan, B.H. Hameed, Development and photocatalytic activities of TiO<sub>2</sub> doped with Ca-Ce-W in the degradation of acid red 1 under visible light irradiation, *Desalination Water Treat.* 52 (2013) 5639–5651, <https://doi.org/10.1080/19443994.2013.813009>.
- [42] W. Ahmad, U. Mehmood, A. Al-Ahmed, F.A. Al-Sulaiman, M.Z. Aslam, M.S. Kamal, R.A. Shawabkeh, Synthesis of zinc oxide/titanium dioxide (ZnO/TiO<sub>2</sub>) nanocomposites by wet impregnation versus impregnation method and preparation of ZnO/TiO<sub>2</sub> paste using poly(vinylpyrrolidone) for efficient dye-sensitized solar cells, *Electrochim. Acta* 222 (2016) 473–480, <https://doi.org/10.1016/j.electacta.2016.10.200>.
- [43] J. Chen, W. Liao, Y. Jiang, D. Yu, M. Zou, H. Zhu, M. Zhang, M. Du, Facile fabrication of ZnO/TiO<sub>2</sub> heterogeneous nanofibres and their photocatalytic behaviour and mechanism towards rhodamine B, *Nanomater. Nanotechnol.* 6 (2016) 1–8, <https://doi.org/10.5772/62291>.
- [44] U.G. Akpan, B.H. Hameed, Desalination and Water Treatment Development and photocatalytic activities of TiO<sub>2</sub> doped with Ca-Ce-W in the degradation of acid red 1 under visible light irradiation, *Desalination Water Treat.* 52 (2014) 5639–5651, <https://doi.org/10.1080/19443994.2013.813009>.
- [45] J. Arin, S. Thongtem, A. Phuruangrat, T. Thongtem, Template synthesis of Zn<sub>2</sub>TiO<sub>4</sub> and Zn<sub>2</sub>Ti<sub>3</sub>O<sub>8</sub> nanorods by hydrothermal-calcination combined processes, *Mater. Lett.* 193 (2017) 270–273, <https://doi.org/10.1016/j.matlet.2017.01.142>.
- [46] C. Wang, W. Hwang, K. Chang, H. Ko, C. Hsi, Formation and morphology of Zn<sub>2</sub>Ti<sub>3</sub>O<sub>8</sub> powders using hydrothermal process without dispersant agent or mineralizer, *Int. J. Mol. Sci.* 12 (2011) 935–945, <https://doi.org/10.3390/ijms12020935>.

- [47] Y.S. Chang, Y.H. Chang, I. Chen, G.J. Chen, Y.L. Chai, T.H. Fang, S. Wu, Synthesis, formation and characterization of ZnTiO<sub>3</sub> ceramics, *Ceram. Int.* 30 (2004) 2183–2189, <https://doi.org/10.1016/j.ceramint.2004.01.002>.
- [48] A. Habib, T. Shahadat, N.M. Bahadur, I.M.I. Ismail, A.J. Mahmood, Synthesis and characterization of ZnO-TiO<sub>2</sub> nanocomposites and their application as photocatalysts, *Int. Nano Lett.* 3 (2013) 1–8, <https://doi.org/10.1186/2228-5326-3-5>.
- [49] Z.A. Allothman, A review: fundamental aspects of silicate mesoporous materials, *Materials* 5 (2012) 2874–2902, <https://doi.org/10.3390/ma5122874>.
- [50] N. Nasuha, S. Ismail, B.H. Hameed, Activated electric arc furnace slag as an efficient and reusable heterogeneous Fenton-like catalyst for the degradation of Reactive Black 5, *J. Taiwan Inst. Chem. Eng.* 67 (2016) 235–243, <https://doi.org/10.1016/j.jtice.2016.07.023>.
- [51] G. Prados-Joya, M. Sánchez-Polo, J. Rivera-Utrilla, M. Ferro-garcía, Photodegradation of the antibiotics nitroimidazoles in aqueous solution by ultraviolet radiation, *Water Res.* 45 (2011) 393–403, <https://doi.org/10.1016/j.watres.2010.08.015>.
- [52] H.-Y. Xu, L.-C. Wu, H. Zhao, L.-G. Jin, S.-Y. Qi, Synergic effect between adsorption and photocatalysis of metal-free g-C<sub>3</sub>N<sub>4</sub> derived from different precursors, *PLoS One* 10 (2015) 1–20, <https://doi.org/10.1371/journal.pone.0142616>.
- [53] U.G. Akpan, B.H. Hameed, Parameters affecting the photocatalytic degradation of dyes using TiO<sub>2</sub>-based photocatalysts: a review, *J. Hazard Mater.* 170 (2009) 520–529, <https://doi.org/10.1016/j.jhazmat.2009.05.039>.
- [54] P. Nuengmatcha, P. Porrawatkul, S. Chanthai, P. Sricharoen, N. Limchoowong, Enhanced photocatalytic degradation of methylene blue using Fe<sub>2</sub>O<sub>3</sub>/graphene/CuO nanocomposites under visible light, *J. Environ. Chem. Eng.* 7 (2019) 103438, <https://doi.org/10.1016/j.jece.2019.103438>.
- [55] R.M. Mohamed, A.A. Ismail, M.W. Kadi, D.W. Bahnemann, A comparative study on mesoporous and commercial TiO<sub>2</sub> photocatalysts for photodegradation of organic pollutants, *J. Photochem. Photobiol. Chem.* 367 (2018) 66–73, <https://doi.org/10.1016/j.jphotochem.2018.08.019>.
- [56] J. Zhang, L. Li, Y. Li, C. Yang, H<sub>2</sub>SO<sub>4</sub> induced mesoporous TiO<sub>2</sub> nano-photocatalyst synthesized free of template under microwave, *Powder Technol.* 335 (2018) 54–61, <https://doi.org/10.1016/j.powtec.2018.05.007>.
- [57] S. Pourmoslemi, A. Mohammadi, F. Kobarfard, M. Amini, Photocatalytic removal of doxycycline from aqueous solution using ZnO nano-particles: a comparison between UV-C and visible light, *Water Sci. Technol.* 74 (2016) 1658–1670, <https://doi.org/10.2166/wst.2016.339>.
- [58] M. Brigante, M. Avena, Biotemplated synthesis of mesoporous silica for doxycycline removal. Effect of pH, temperature, ionic strength and Ca<sup>2+</sup> concentration on the adsorption behaviour, *Microporous Mesoporous Mater.* 225 (2016) 534–542, <https://doi.org/10.1016/j.micromeso.2016.01.035>.
- [59] B.H. Diya'Uddeen, W.M.A.W. Daud, A.R. Abdul Aziz, Treatment technologies for petroleum refinery effluents: a review, *Process Saf. Environ. Protect.* 89 (2011) 95–105, <https://doi.org/10.1016/j.psep.2010.11.003>.
- [60] D.-C. He, Q.-M. Fu, Z.-B. Ma, H.-Y. Zhao, Y.-F. Tu, Y. Tian, G. Zheng, H.-B. Lu, Facile synthesis and photocatalytic activity of ZnO/zinc titanate core-shell nanorod arrays, *Mater. Res. Express* (2018), <https://doi.org/10.1016/j.colex.2018.10.012>.
- [61] W. Liu, J. Zhou, Z. Hu, Nano-sized g-C<sub>3</sub>N<sub>4</sub> thin layer @ CeO<sub>2</sub> sphere core-shell photocatalyst combined with H<sub>2</sub>O<sub>2</sub> to degrade doxycycline in water under visible light irradiation, *Sep. Purif. Technol.* 227 (2019) 1–10, <https://doi.org/10.1016/j.seppur.2019.06.003>.
- [62] J. Gao, Y. Gao, Z. Sui, Z. Dong, S. Wang, D. Zou, Hydrothermal synthesis of BiOBr/FeWO<sub>4</sub> composite photocatalysts and their photocatalytic degradation of doxycycline, *J. Alloys Compd.* 732 (2018) 43–51, <https://doi.org/10.1016/j.jallcom.2017.10.092>.
- [63] D. Klauson, M. Sakarašvili, N. Pronina, M. Krichevskaya, E. Kärber, V. Mikli, Aqueous photocatalytic degradation of selected micropollutants by Pd-modified titanium dioxide in three photoreactor types, *Environ. Technol.* 38 (2017) 860–871, <https://doi.org/10.1080/09593330.2016.1214185>.
- [64] P. Hong, Y. Li, J. He, A. Saeed, K. Zhang, C. Wang, L. Kong, J. Liu, Rapid degradation of aqueous doxycycline by surface CoFe<sub>2</sub>O<sub>4</sub>/H<sub>2</sub>O<sub>2</sub> system: behaviors, mechanisms, pathways and DFT calculation, *Appl. Surf. Sci.* 526 (2020) 146557, <https://doi.org/10.1016/j.apsusc.2020.146557>.
- [65] F. Berdini, J.O. Otalvaro, M. Avena, M. Brigante, Photodegradation of doxycycline in water induced by TiO<sub>2</sub>-MCM-41. Kinetics, TOC evolution and reusability, *Results in Engineering* 16 (2022) 100765, <https://doi.org/10.1016/j.rineng.2022.100765>.
- [66] Q. Wu, Y. Song, Enhanced interfacial charge migration through fabrication of p-n junction in ZnIn<sub>2</sub>S<sub>4</sub>/NiFe<sub>2</sub>O<sub>4</sub>/biochar composite for photocatalytic doxycycline hydrochloride degradation, *Chem. Eng. J.* 453 (2023) 139745, <https://doi.org/10.1016/j.cej.2022.139745>.
- [67] Y. Yu, D. Chen, W. Xu, J. Fang, J. Sun, Z. Liu, Y. Chen, Y. Liang, Z. Fang, Synergistic adsorption-photocatalytic degradation of different antibiotics in seawater by a porous g-C<sub>3</sub>N<sub>4</sub>/calcin-LDH and its application in synthetic mariculture wastewater, *J. Hazard Mater.* 416 (2021) 126183, <https://doi.org/10.1016/j.jhazmat.2021.126183>.
- [68] S. Swetha, M.A. Abdel-Maksoud, M.K. Okla, B. Janani, T.M. Dawoud, M.A. El-Tayeb, S. Sudheer Khan, Triple-mechanism driven Fe-doped n-n hetero-architecture of Pr<sub>6</sub>O<sub>11</sub>-MoO<sub>3</sub> decorated g-C<sub>3</sub>N<sub>4</sub> for doxycycline degradation and bacterial photoinactivation, *Chem. Eng. J.* 461 (2023) 141806, <https://doi.org/10.1016/j.cej.2023.141806>.